Figure 11 $S21$ of measurement

power at 37.5GHz. And the phase of output ports agreed with the results shown in Figure 5.

3. EXPERIMENT RESULT

A QO power divider were fabricated practically and the S-parameter was measured at 37.5GHz using a Millimeter wave vector network analyzer (37369C, Anritsu). The measured transmission coefficients between all output ports and input port are shown in Figure 11. The insertion loss variation of different output ports was less than ± 2.1 dB and the relative phase variation less than $9°$. Total output power was achieved by adding up the power of all out ports to be 80.8% of the input power at the designed working frequency, which is well agreed with the simulated value of 88.7%.

4. CONCLUSIONS

A general method of designing QO power divider was proposed in this article. And applying this method, a 1×18 QO power divider was designed successfully. The measured results of the divider were consistent with that of simulation, and the ratio of the total output power to the input power was 80.8%. So feasibility of holography QO power-combining was verified and validity of method of designing was also confirmed by the experiment.

Divider to split input power into further more outputs directly can be designed using this method. And this method can be used to solve the heat-sinking problem at higher frequencies even at submillimeter wave band because of no degradation of dividing efficiency resulted by enlarging spacing between neighbor output ports.

REFERENCES

1. R.A. York, Some considerations for optimal efficiency and low noise in large power combiners, IEEE Trans Microwave Theory Tech 49 (2001), 1477–1482.
2. D.B. Rutledge, N.S. Cheng, R.A. York, R.M. Weikle, II, and M.P. DeLisio, Failures in power-combining arrays, IEEE Trans Microwave Theory Tech 47 (1999), 1077–1082.
3. T. Magath, Diffraction synthesis and experimental verification of a quasi-optical power splitter at 150 GHzIEEE, Trans Microwave Theory Tech 52 (2004).
4. T. Magath, M. Höft, and R. Judaschke, A two-dimensional quasi-optical power combining oscillator array with external injection locking, IEEE Trans Microwave Theory Tech 52 (2004).
5. R. Judaschke, M. Hoft, and K. Schunemann, Quasi-optical 150-GHz power combining oscillator. IEEE Microwave Wirel Compon Lett 15 (2005).
6. M.G. Keller, J. Shaker, and Y.M.M. Antar, Millimeter-wave talbot array illuminators, Antennas Wirel Propag Lett 5 (2006).
7. D.B. Rensch, R.A. York, N.-S. Cheng, P. Jia, A 120-W-band spatially combined solid-state amplifier, IEEE Trans Microwave Theory Tech 47 (1999).
8. P. Jia, L.-Y. Chen, A. Alexanian, and R.A. York, Broad-band high-power amplifier using spatial power-combining technique, IEEE Trans Microwave Theory Tech 51 (2003).
9. H.F. Talbot, Facts relating to optical science, Phillos Mag 9 (1836), 403–405.
10. A.W. Lohmann and J.A. Thomas, Making an array illuminator based on the Talbot effect, Appl Opt 29 (1990), 4337–4340.
11. L. Rayleigh, On copying diffraction gratings and on some phenomenon connected therewith, Philos Mag 11 (1881), 196.
12. J.T. Winthorp and C.R. Worthington, Theory of Fresnel images. I. Plane periodic objects in monchromatic light, J Opt Soc Am 55 (1965), 657–661.
13. W. Klaus, Y. Hamaguchi, K. Kodate, and Y. Arimoto, Theoretical and experimental evaluation of waveguide Talbot array illuminators, SPIE 3010 (1997).

ON-BOARD SMALL-SIZE PRINTED LTE/WWAN MOBILE HANDSET ANTENNA CLOSELY INTEGRATED WITH SYSTEM GROUND PLANE

Fang-Hsien Chu and Kin-Lu Wong

Department of Electrical Engineering, National Sun Yat-sen University, Kaohsiung 80424, Taiwan; Corresponding author: wongkl@ema.ee.nsysu.edu.tw

ABSTRACT: *An on-board uniplanar printed mobile handset antenna with a small size of 15×30 mm^2 for 8-band long term evolution/wireless wide area network (LTE/WWAN) (698–960/1710–2690 MHz) operation is presented. The antenna is a spiral monopole coupled with a long parasitic shorted strip. The spiral monopole has a length of 78 mm (about 0.25 wavelength at 950 MHz), while the shorted strip capacitively excited by the spiral monopole has a length of 125 mm (close to 0.25 wavelength at 700 MHz). The spiral monopole is encircled by the shorted strip so that the antenna has a compact configuration to fit in a small no-ground portion at the corner of the bottom edge of the main circuit board in the mobile handset. In addition, the antenna is closely integrated with the system ground plane on the main circuit board and is spaced by a small distance of 0.5 mm to the nearby system ground plane. This leads to compact integration of the on-board LTE/WWAN printed antenna on the main circuit board of the mobile handset. Results of the proposed antenna including its specific absorption rate and hearing aid compatibility behavior are presented and discussed. The antenna is about the smallest for the on-board all-printing LTE/WWAN handset antennas that have been reported for the present.* © 2011 Wiley Periodicals, Inc. Microwave Opt Technol Lett 53:1336–1343, 2011; View this article online at wileyonlinelibrary.com. DOI 10.1002/mop.25961

Key words: *mobile antennas; handset antennas; LTE antennas; WWAN antennas; on-board printed handset antennas*
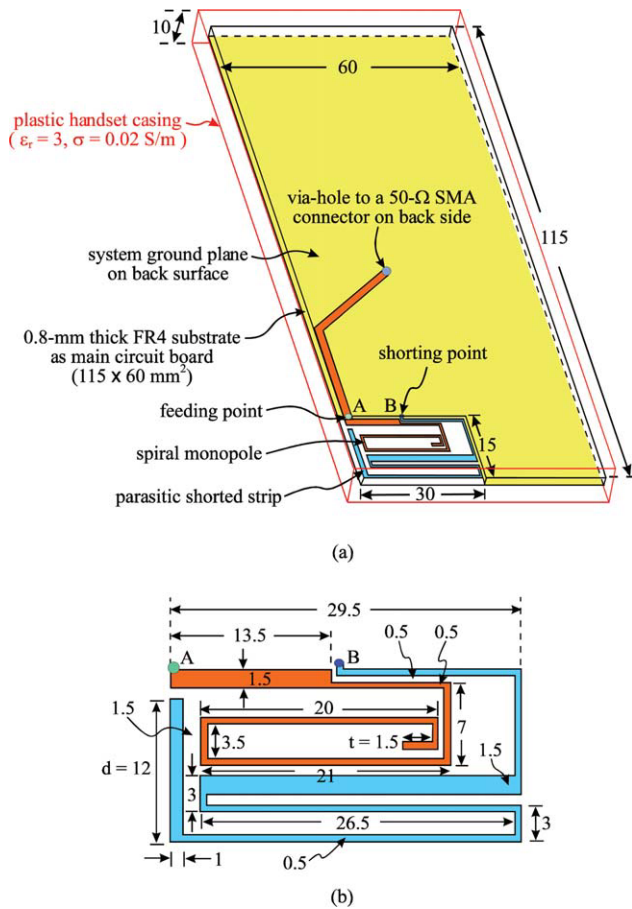
Figure 1 (a) Geometry of the on-board printed LTE/WWAN mobile handset antenna closely integrated with system ground plane. (b) Dimensions of the antenna. [Color figure can be viewed in the online issue, which is available at wileyonlinelibrary.com]

1. INTRODUCTION

The on-board printed internal antenna with a two-dimensional structure is easy to fabricate and very suitable for slim mobile handset applications, owing to its very low profile compared with the traditional three-dimensional bulk internal antennas [1–5]. There have been some promising on-board printed antennas reported for the five-band wireless wide area network (WWAN) operation in the 824–960 and 1710–2690 MHz bands [6–13]. For covering eight-band long term evolution (LTE) [14]/ WWAN operation in the 698–960 MHz band (LTE700/ GSM850/900) and 1710–2690 MHz band (GSM1800/1900/ UMTS/LTE2300/2500), relatively few designs have been demonstrated [15–18], owing to the design challenge to obtain a much wider operating band with a small board space occupied for the antenna. For the present, the reported eight-band LTE/ WWAN internal mobile handset antennas [15–18] are required to be disposed at the entire top or bottom edge of the main circuit board of the mobile handset. The required antenna size causes a problem in integrating the antenna with the associated elements such as the universal series connector (USB) connector [19] as a data port of the mobile handset or the loudspeaker [20, 21] or the lens of the embedded digital camera [22–24] on the main circuit board and limits the compact integration of the LTE/WWAN antenna inside the mobile handset.

In this article, we present an on-board printed internal mobile handset antenna for eight-band LTE/WWAN operation with a
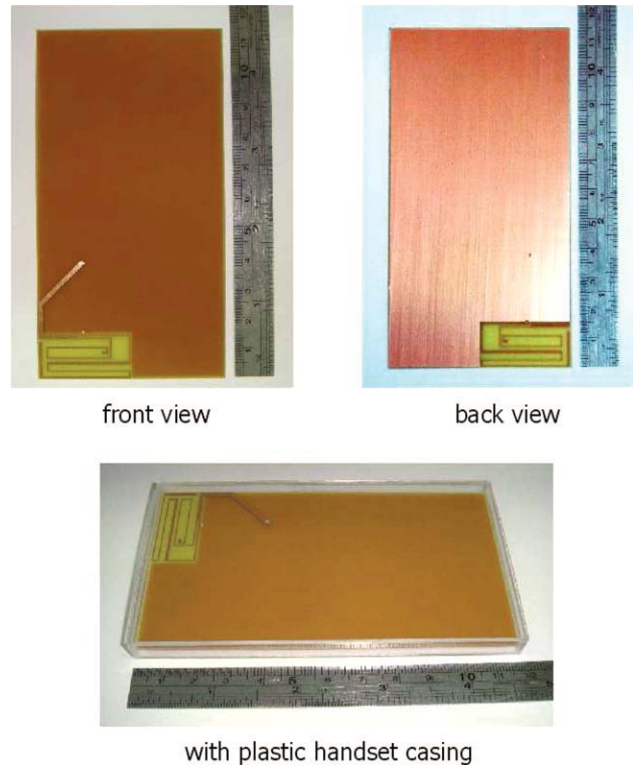
Figure 2 Photos of the fabricated antenna. [Color figure can be viewed in the online issue, which is available at wileyonlinelibrary.com]

small printing size of 15×30 mm², which is about the smallest for the on-board all-printing LTE/WWAN handset antennas that have been reported for the present. The antenna is formed by a spiral monopole encircled by a long parasitic shorted strip, which is spaced with a small distance of 0.5 mm to the nearby system ground plane on the main circuit board of the mobile handset. Since the antenna is capable of being in close proximity to the nearby system ground plane, it decreases the required board space for the proposed antenna. Also, the spiral monopole and the parasitic shorted strip can both contribute wideband resonant modes for the antenna's lower and upper bands, thereby leading to wideband operating bands for the antenna to cover eight-band LTE/WWAN operation. Detailed operating principle
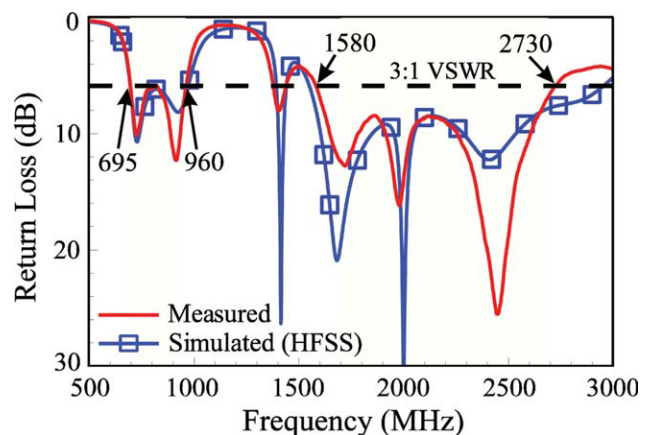
Figure 3 Measured and simulated return loss of the fabricated antenna. [Color figure can be viewed in the online issue, which is available at wileyonlinelibrary.com]
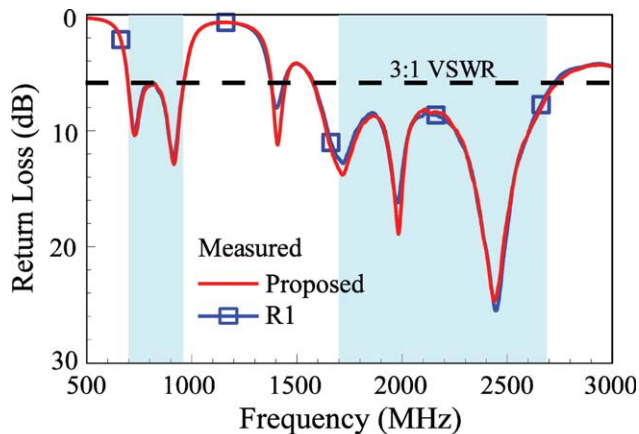
Figure 4 Measured return loss of the fabricated antenna with the presence of a nearby USB connector. [Color figure can be viewed in the online issue, which is available at wileyonlinelibrary.com]

of the proposed antenna is described in the article. Results of the fabricated prototype of the proposed antenna are presented and discussed. The radiation characteristics including the SAR [25–27] and hearing aid compatibility (HAC) [28–31] behavior of the proposed antenna are also analyzed.

2. PROPOSED ANTENNA

Figure 1(a) shows the geometry of the proposed antenna, and Figure 1(b) gives the dimensions of the metal pattern of the antenna. The antenna is printed on one corner of the bottom edge of the main circuit board, which is an FR4 substrate (relative permittivity 4.4 and conductivity 0.02 S/m) of length 115 mm and width 60 mm in the study. The antenna occupies a no-ground region of size 15×30 mm^2. On the same side of the
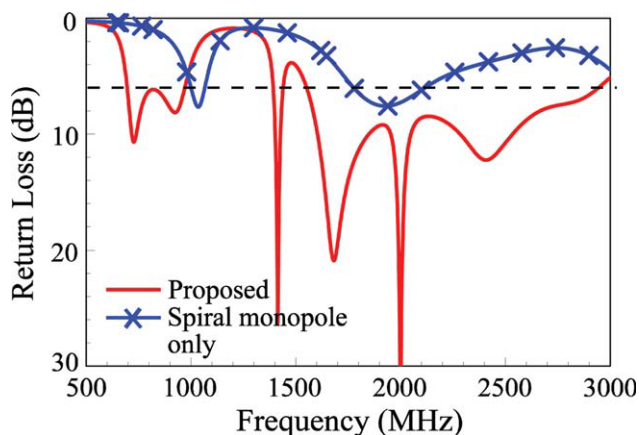
Figure 5 Simulated return loss for the proposed antenna (the spiral monopole and the parasitic shorted strip) and the spiral monopole only. [Color figure can be viewed in the online issue, which is available at wileyonlinelibrary.com]

main circuit board, a ground plane is printed, which encloses the proposed antenna with a small distance of 0.5 mm. The close proximity of the proposed on-board printed antenna to the nearby system ground plane leads to compact integration of the internal antenna on the main circuit board. This can also lead to efficient circuit layout planning on the main circuit board.

The antenna is with a two-dimensional planar structure, allowing it easy to fabricate on the main circuit board. The antenna comprises a spiral monopole and a long parasitic shorted strip, with the spiral monopole encircled by the parasitic shorted strip to achieve a compact configuration. The spiral monopole has a length of 78 mm, which is about 0.25 wavelength at 950 MHz. The feeding point A of the spiral monopole is also the antenna's feeding point. In the experiment to test the antenna, a 50-Ω microstrip line of about 30 mm is printed on the main circuit board and further connected through a via-hole in the circuit board to a 50-Ω SMA connector located at the back side of the circuit board.

The parasitic shorted strip has a longer length of 125 mm, which is close to 0.25 wavelength at 700 MHz. Both the spiral monopole and parasitic shorted strip contribute their fundamental resonant modes to form a wide operating band at about 900
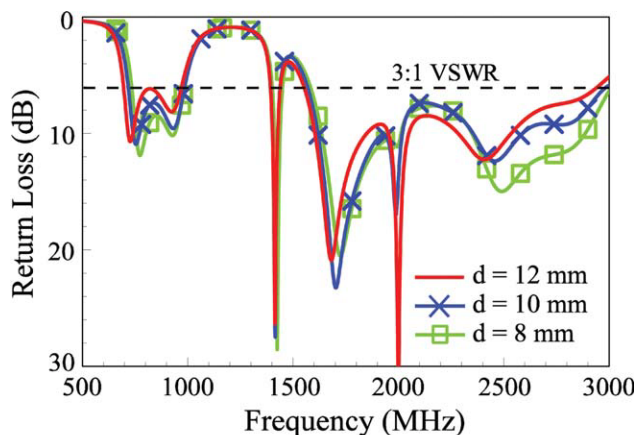
(a)
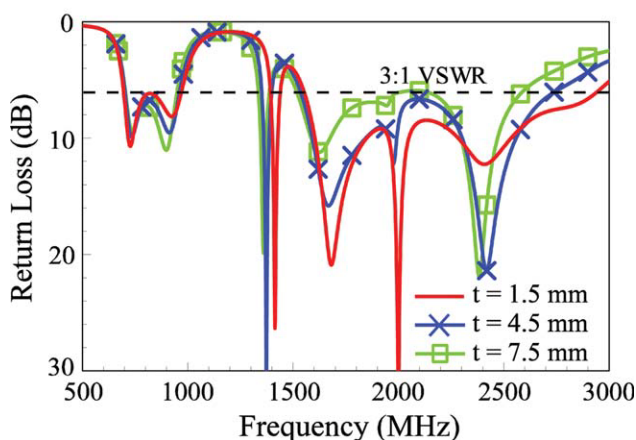
(b)

Figure 6 Simulated return loss for the proposed antenna as a function of (a) the end-section length d of the parasitic shorted strip and (b) the end-section length t of the spiral monopole. Other dimensions are the same as given in Fig. 1. [Color figure can be viewed in the online issue, which is available at wileyonlinelibrary.com]
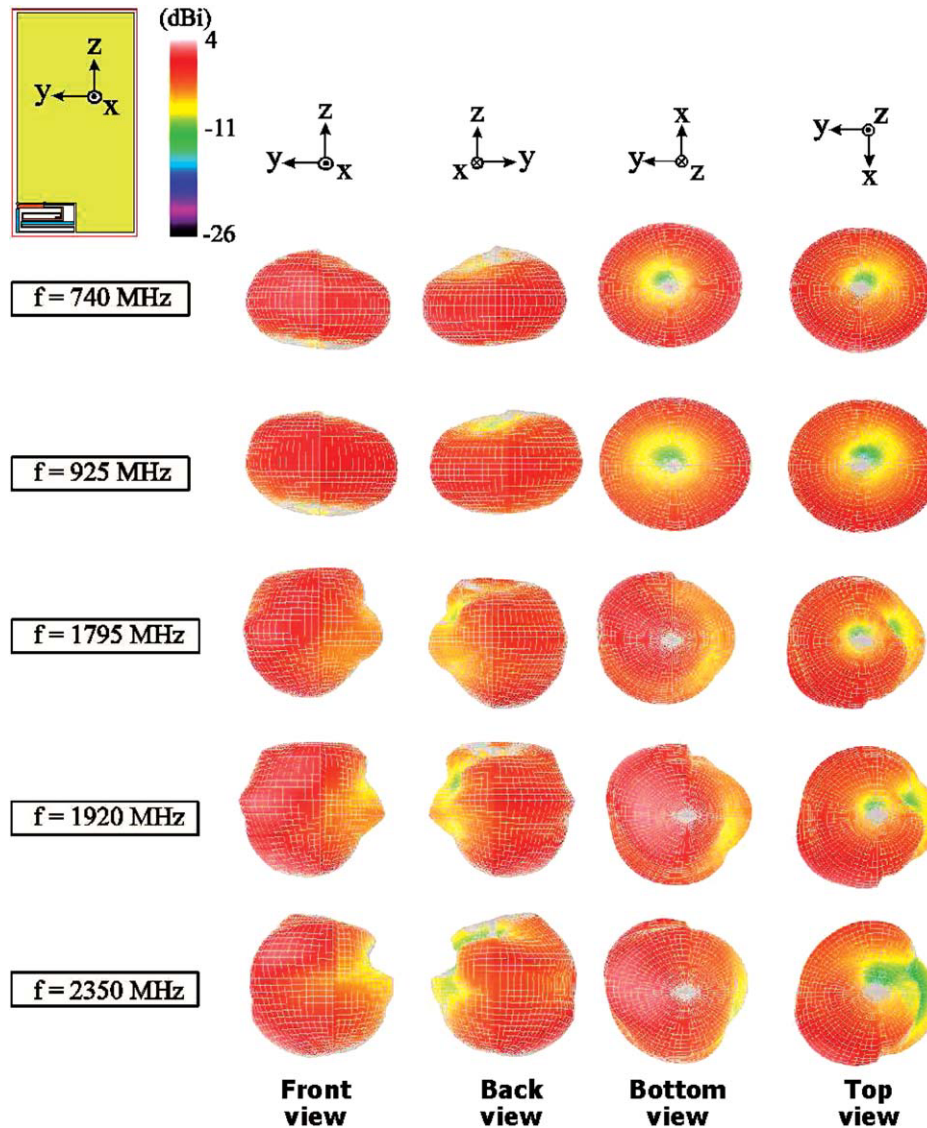
Figure 7 Measured three-dimensional total-power radiation patterns for the proposed antenna. [Color figure can be viewed in the online issue, which is available at wileyonlinelibrary.com]

MHz to cover the LTE700/GSM850/900 operation. The higher-order resonant modes of the spiral monopole and parasitic shorted strip are also combined into a wide operating band for the antenna to cover the GSM1800/1900/UMTS/LTE2300/2500 operation. Also note that the parasitic shorted strip is capacitively excited by the spiral monopole. Through the capacitive coupling, good excitation of the parasitic shorted strip to generate its fundamental and higher-order resonant modes to enhance the bandwidth of the proposed antenna is obtained in this study.

3. RESULTS AND DISCUSSION

The proposed antenna was fabricated and studied. Figure 2 shows the photos of the fabricated antenna in its front view, back view, and plastic handset casing included. Results of the measured and simulated return loss of the fabricated antenna are presented in Figure 3. The simulated results are obtained using simulation software high frequency structure simulator (HFSS) version 12 [32]. The measured data agree with the HFSS simulated results. From the results, two wide operating bands are obtained. The lower and upper bands, respectively cover the

desired 698–960 and 1710–2690 MHz bands, and eight-band LTE/WWAN operation is achieved.

It should be noted that as the antenna does not require to occupy the entire bottom edge of the main circuit board and can be closely integrated with the nearby ground plane, associated electronic components can be placed at the ground plane close to the antenna. To demonstrate this attractive feature, Figure 4 shows the measured return loss of the fabricated antenna with the presence of a nearby USB connector [19] as a data port of the mobile handset (see the photo in the figure). Results show very small variations in the measured return loss for the two cases with and without a nearby USB connector. This indicates that compact integration of the proposed antenna and the associated electronic components inside the mobile handset can be obtained.

Figure 5 shows a comparison of the simulated return loss for the proposed antenna and the case with the spiral monopole only. It is seen that with the spiral monopole only, there are two resonant modes occurred at about 1000 and 2000 MHz, whose bandwidths are far from covering the desired LTE/WWAN operation. By adding the parasitic shorted strip to form the proposed
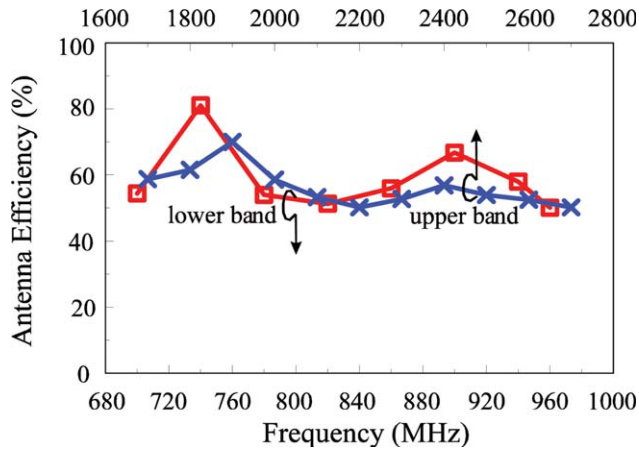
Figure 8 Measured antenna efficiency (mismatching loss included) for the proposed antenna. [Color figure can be viewed in the online issue, which is available at wileyonlinelibrary.com]

antenna, additional resonant modes are provided to widen the bandwidth of the antenna. In the lower band, an additional resonant mode at about 700 MHz contributed by the parasitic shorted strip combines with the one generated by the spiral monopole and shifted to lower frequencies at about 900 MHz to form a wide operating band to cover the LTE700/GSM850/900 operation. Three higher-order resonant modes at about 1700, 2000, and 2450 MHz contributed either by the parasitic shorted strip or spiral monopole are also generated to form a wide oper-

ating band to cover the GSM1800/1900/UMTS/LTE2300/2500 operation. Also note that the resonant mode at about 1400 MHz is generated by the parasitic shorted strip, although it does not contribute to enhance the upper-band bandwidth.

To analyze the excited resonant modes more clearly, Figures 6(a) and 6(b) shows the simulated return loss as a function of the end-section length d of the parasitic shorted strip and the end-section length t of the spiral monopole, respectively. With other dimensions fixed as given in Figure 1, results for the length d varied from 8 to 12 mm are shown in Figure 6(a). Since the variation in the length d changes the resonant length of the parasitic shorted strip, the resonant mode at about 700 MHz mainly contributed by the parasitic shorted strip are shifted to lower frequencies with an increase in the length d. Some variations in the impedance matching level, with the resonant frequency fixed, of the resonant mode at about 950 MHz generated by the spiral monopole are also seen. Results for the length t varied from 1.5 to 7.5 mm are shown in Figure 6(b). Owing to the variations in the length t which changes the resonant length of the spiral monopole, the resonant modes at about 950 MHz generated by the spiral monopole are shifted to lower frequencies with an increase in the length t. At the same time, small effects on the resonant modes at about 700 MHz controlled by the parasitic shorted strip are seen. For the resonant modes in the upper band, impedance matching variations in the 1700, 2000, and 2045 MHz are seen when either the length d or t is varied. This is largely because there are strong coupling between the spiral monopole and parasitic shorted strip, and some variations in either the length d or t will hence cause some strong
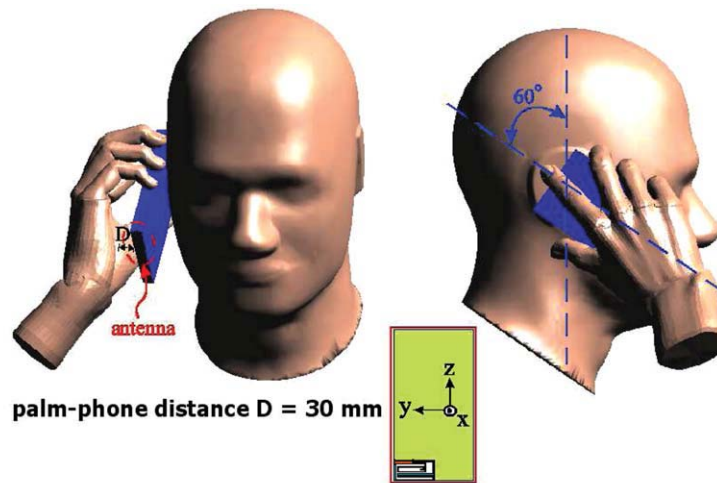
Frequency (MHz)	Testing power (dBm)	SAR, head only (W/kg)	Return Loss, head only (dB)	SAR, head and hand (W/kg)	Return Loss, head and hand (dB)
740	21	0.32	8.7	0.26	8.7
859	24	0.85	7.4	0.68	5.8
925	24	0.90	7.6	0.77	6.4
1795	21	0.37	10.5	1.22	11.2
1920	21	0.37	7.9	0.91	7.1
2045	21	0.32	14.5	0.85	16.5
2350	21	0.43	12.7	0.76	10.0
2595	21	0.40	8.9	1.24	8.6

Figure 9 SAR simulation model and the simulated 1-g SAR values for the proposed antenna. [Color figure can be viewed in the online issue, which is available at wileyonlinelibrary.com]
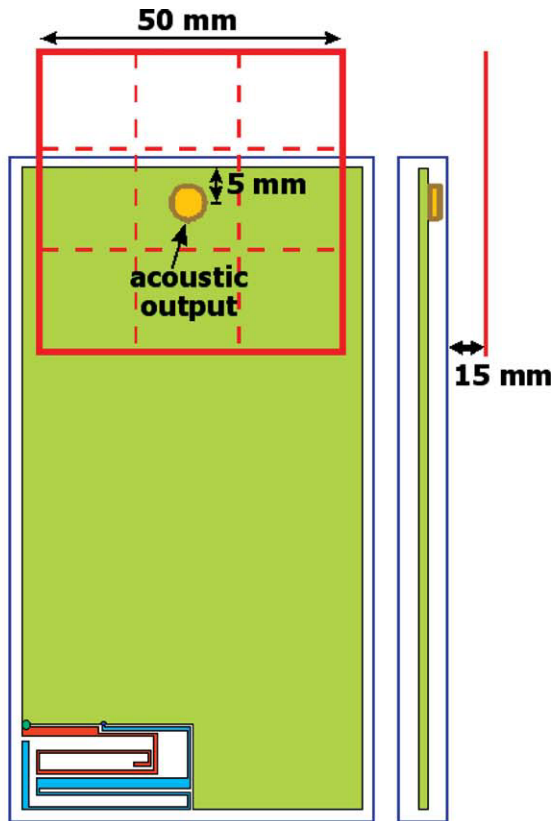
Frequency (MHz)	Testing power (dBm)	E-field (V/m in dB)		H-field (A/m in dB)	
740	21	34.8	M4	-21.9	M4
859	33	47.5	M3	-7.9	M4
925	33	47.1	M3	-7.7	M4
1795	30	38.4	M3	-11.4	M2
1920	30	39.5	M2	-11.1	M2
2045	21	30.0	M4	-20.1	M4
2350	21	31.2	M4	-18.8	M4
2595	21	31.2	M4	-18.7	M4

Figure 10 HAC simulation model and the simulated HAC values for the proposed antenna. [Color figure can be viewed in the online issue, which is available at wileyonlinelibrary.com]

effects on the higher-order resonant modes contributed either by the spiral monopole and parasitic shorted strip.

Figure 7 shows the three-dimensional total-power radiation patterns for the proposed antenna measured in a far-field anechoic chamber. Results at typical frequencies of 740, 925, 1795, 1920, and 2350 MHz are presented. At 740 and 925 MHz in the lower band, half-wavelength dipole-like radiation patterns with omnidirectional radiation in the azimuthal plane (x-y plane) are observed. At 1795, 1920, and 2350 MHz, the radiation patterns are close to full-wavelength dipole-like patterns with some dips in the azimuthal plane. Figure 8 shows the measured antenna efficiency (mismatching loss included) for the antenna. The antenna efficiency varies from about 50 to 80% in the lower band and about 50 to 70% in the upper band. The obtained far-field radiation characteristics are acceptable for practical handset applications.

The near-field radiation characteristics are also studied. Figure 9 shows the SAR simulation model provided by the simulation software SEMCAD version 14 [33] and the simulated 1-g SAR values for the antenna. Both the cases of head only and head and hand are studied. The return loss and testing power at each testing frequency are also given in the table. The obtained SAR values are all less than 1.6 W/kg [25], indicating that the antenna is promising for practical handset applications.

Figure 10 shows the HAC simulation model provided by SEMCAD version 14 [33] and the simulated HAC values for the antenna. The maximum near-field E-field and H-field strengths obtained on the 50×50 mm^2 observation plane centered 15 mm above the acoustic output center at the handset casing are listed in the table in the figure. All the frequencies except at 1795 and 1920 MHz show acceptable HAC results (the field strength in category M3 or M4). The E-field strength

(a)

(b)
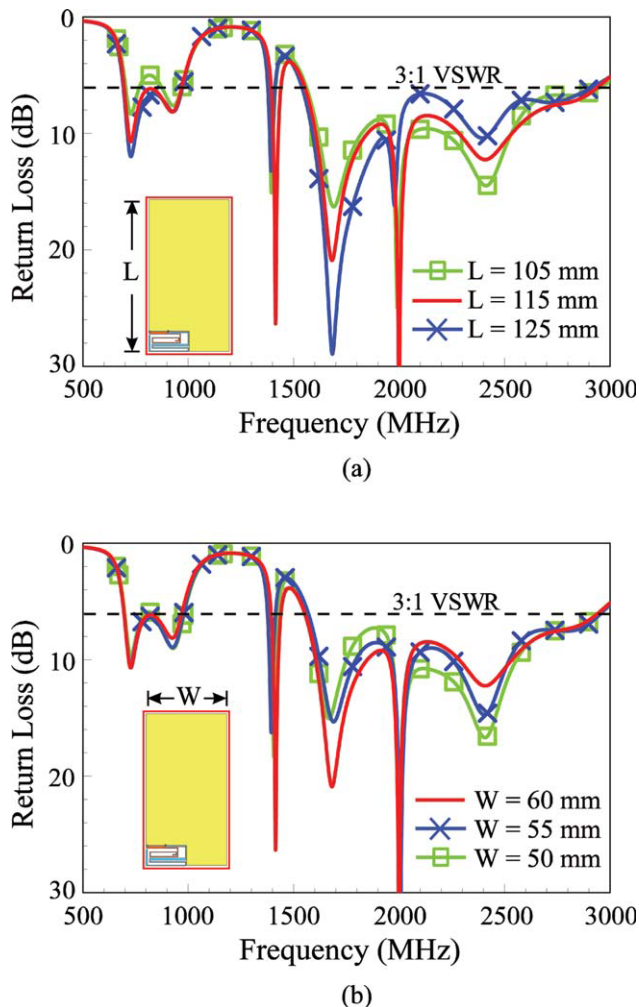
Figure 11 Simulated return loss for the proposed antenna as a function of (a) the length L and (b) the width W of the main circuit board. Other dimensions are the same as in Figure 1. [Color figure can be viewed in the online issue, which is available at wileyonlinelibrary.com]

at 1920 MHz is 39.5 dBV/m and 1.0 dB larger than the limit (38.5 dB) of category M3 for GSM1800 operation. The H-field strengths at 1795 and 1920 MHz are respectively -11.4 and -11.2 dBA/m and larger than the limit (-11.9 dB) of category M3 for GSM1800/1900 operation by 0.5 and 0.7 dB. Since the HAC value is only 1.0 dB or less larger than the limit of category M3 at 1795 and 1920 MHz, it is possible for the proposed antenna to meet the HAC standard for practical applications, because there are usually lossy electronic components nearby the antenna in practical handsets which may lead to decreased near-field emission for the antenna.

Finally, effects of the length and width of the main circuit board on the performance of the antenna are studied. Figure 11(a) shows the simulated return loss for the length L varied from 105 to 125 mm, while the results for the width W varied from 50 to 65 mm are shown in Figure 11(b). For the width variation, the obtained bandwidths for the antenna's lower and upper bands are almost the same. For the length variation, larger effects on the obtained bandwidth are seen for $L = 105$ mm. That is, smaller length of the main circuit board or the system ground plane will lead to decreased bandwidth for the internal WWAN antenna, especially in the lower band at about 900 MHz. This behavior is similar to the chassis effects on the con-

ventional internal WWAN antennas [34, 35]. To improve the antenna's bandwidth due to the smaller length in the main circuit board which decreases the achievable bandwidth of the antenna, the technique of using a small-size inductively coupled patch added at the opposite edge of the main circuit board of the handset can be applied [12]. This technique can lead to enhanced bandwidth for the antenna.

4. CONCLUSION

An all-printing uniplanar antenna directly disposed on the main circuit board of the mobile handset and closely integrated with nearby system ground plane for eight-band LTE/WWAN operation has been proposed. The printing area of the antenna on the main circuit board is 15×30 mm^2 only, and two wide operating bands of 698–960 and 1710–2690 MHz are obtained to cover eight-band LTE/WWAN operation. Small size of the antenna is obtained by compact integration of a spiral monopole and a parasitic shorted strip, while wideband operation is achieved by efficient capacitive coupling between the spiral monopole and parasitic shorted strip. Detailed operating principle has been analyzed in the article. Far-field radiation characteristics of the antenna have been studied, which are acceptable for practical handset applications. Near-field emission of the antenna such as the SAR and HAC results has also been analyzed. The 1-g SAR results over the eight operating bands meet the limit of 1.6 W/kg for practical applications. The HAC results suggest that the antenna is very possible to operate as a hearing-aid compatible mobile device when the antenna is applied in practical mobile handsets.

REFERENCES

1. R.A. Bhatti, Y.T. Im, and S.O. Park, Compact PIFA for mobile terminals supporting multiple cellular and non-cellular standards, IEEE Trans Antennas Propagat 57 (2009), 2534–2540.
2. A. Cabedo, J. Anguera, C. Picher, M. Ribo, and C. Puente, Multiband handset antenna combining a PIFA, slots, and ground plane modes, IEEE Trans Antennas Propagat 57 (2009), 2526–2533.
3. C.L. Liu, Y.F. Lin, C.M. Liang, S.C. Pan, and H.M. Chen, Miniature internal penta-band monopole antenna for mobile phones, IEEE Trans Antennas Propagat 58 (2010), 1008–1011.
4. M.Z. Azad and M. Ali, A miniaturized Hilbert PIFA for dual-band mobile wireless applications, IEEE Antennas Wireless Propagat Lett 4 (2005), 59–62.
5. Y.X. Guo, M.Y.W. Chia, and Z.N. Chen, Miniature built-in multiband antennas for mobile handsets, IEEE Trans Antennas Propagat 52 (2004), 1936–1944.
6. C.I. Lin and K.L. Wong, Printed monopole slot antenna for internal multiband mobile phone antenna, IEEE Trans Antennas Propagat 55 (2007), 3690–3697.
7. C.H. Chang and K.L. Wong, Printed $\lambda/8$-PIFA for penta-band WWAN operation in the mobile phone, IEEE Trans Antennas Propagat 57 (2009), 1373–1381.
8. C.T. Lee and K.L. Wong, Uniplanar coupled-fed printed PIFA for WWAN/WLAN operation in the mobile phone, Microwave Opt Technol Lett 51 (2009), 1250–1257.
9. C.T. Lee and K.L. Wong, Internal WWAN clamshell mobile phone antenna using a current trap for reduced groundplane effects, IEEE Trans Antennas Propagat 57 (2009), 3303–3308.
10. F.H. Chu and K.L. Wong, Simple folded monopole slot antenna for penta-band clamshell mobile phone application, IEEE Trans Antennas Propagat 57 (2009), 3680–3684.
11. K.L. Wong and S.C. Chen, Printed single-strip monopole using a chip inductor for penta-band WWAN operation in the mobile phone, IEEE Trans Antennas Propagat 58 (2010), 1011–1014.
12. C.H. Chang and K.L. Wong, Bandwidth enhancement of internal WWAN antenna using an inductively coupled plate in the small-

size mobile phone, Microwave Opt Technol Lett 52 (2010), 1247–1253.

13. K.L. Wong and C.H. Chang, On-board small-size printed monopole antenna integrated with USB connector for penta-band WWAN mobile phone, Microwave Opt Technol Lett 52 (2010), 2523–2527.

14. http://en.wikipedia.org/wiki/3GPP_Long_Term_Evolution.

15. C.T. Lee and K.L. Wong, Planar monopole with a coupling feed and an inductive shorting strip for LTE/GSM/UMTS operation in the mobile phone, IEEE Trans Antennas Propagat 58 (2010), 2478–2483.

16. K.L. Wong, M.F. Tu, C.Y. Wu, and W.Y. Li, Small-size coupled-fed printed PIFA for internal eight-band LTE/GSM/UMTS mobile phone antenna, Microwave Opt Technol Lett 52 (2010), 2123–2128.

17. S.C. Chen and K.L. Wong, Bandwidth enhancement of coupled-fed on-board printed PIFA using bypass radiating strip for eight-band LTE/GSM/UMTS slim mobile phone, Microwave Opt Technol Lett 52 (2010), 2059–2065.

18. K.L. Wong, W.Y. Chen, C.Y. Wu, and W.Y. Li, Small-size internal eight-band LTE/WWAN mobile phone antenna with internal distributed LC matching circuit, Microwave Opt Technol Lett 52 (2010), 2244–2250.

19. http://en.wikipedia.org/wiki/Universal_Serial_Bus, Wikipedia.

20. C.H. Wu and K.L. Wong, Internal shorted planar monopole antenna embedded with a resonant spiral slot for penta-band mobile phone application, Microwave Opt Technol Lett 50 (2008), 529–536.

21. Y.W. Chi and K.L. Wong, Half-wavelength loop strip fed by a printed monopole for penta-band mobile phone antenna, Microwave Opt Technol Lett 50 (2008), 2549–2554.

22. K.L. Wong, S.L. Chien, C.M. Su, and F.S. Chang, An internal planar mobile phone antenna with a vertical ground plane, Microwave Opt Technol Lett 47 (2005), 597–599.

23. C.M. Su, K.L. Wong, C.L. Tang, and S.H. Yeh, EMC internal patch antenna for UMTS operation in a mobile device, IEEE Trans Antennas Propagat 53 (2005), 3836–3839.

24. M.R. Hsu and K.L. Wong, WWAN ceramic chip antenna for mobile phone application, Microwave Opt Technol Lett 51 (2009), 103–110.

25. American National Standards Institute (ANSI), Safety levels with respect to human exposure to radio-frequency electromagnetic field, 3 kHz to 300 GHz, ANSI/IEEE standard C95.1, April 1999.

26. C.H. Li, E. Ofli, N. Chavannes, and N. Kuster, Effects of hand phantom on mobile phone antenna performance, IEEE Trans Antennas Propagat 57 (2009), 2763–2770.

27. Y.W. Chi and K.L. Wong, Compact multiband folded loop chip antenna for small-size mobile phone, IEEE Trans Antennas Propagat 56 (2008), 3797–3803.

28. American National Standard for Method of Measurement of Compatibility between Wireless Communication Devices and Hearing Aids (ANSI C63. 19–2007, revision ANSI C63. 19–2006), American National Standards Institute, New York, 2007.

29. T. Yang, W.A. Davis, W.L. Stutzman, and M.C. Huynh, Cellular-phone and hearing-aid interaction: An antenna solution, IEEE Antennas Propagat Mag 50 (2008), 51–65.

30. W.Y. Chen and K.L. Wong, Wideband coupled-fed PIFA for HAC penta-band clamshell mobile phone, Microwave Opt Technol Lett 51 (2009), 2369–2374.

31. K.L. Wong and M.F. Tu, Hearing aid-compatible internal penta-band antenna for clamshell mobile phone, Microwave Opt Technol Lett 51 (2009), 1408–1413.

32. http://www.ansoft.com/products/hf/hfss/, Ansoft Corporation HFSS, Pittsburgh, PA.

33. http://www.semcad.com, SEMCAD, Schmid & Partner Engineering AG (SPEAG).

34. T.Y. Wu and K.L. Wong, On the impedance bandwidth of a planar inverted-F antenna for mobile handsets, Microwave Opt Technol Lett 32 (2002), 249–251.

35. P. Vainikainen, J. Ollikainen, O. Kivekas, and I. Kelander, Resonator-based analysis of the combination of mobile handset antenna and chassis, IEEE Trans Antennas Propagat 50 (2002), 1433–1444.

ACCURACY–EFFICIENCY TRADEOFF OF TEMPORAL BASIS FUNCTIONS FOR TIME-MARCHING SOLVERS

Guneet Kaur and Ali E. Yilmaz
Department of Electrical and Computer Engineering, University of Texas at Austin, Austin, TX; Corresponding author: guneet@mail.utexas.edu

ABSTRACT: *An investigation of the impact of the temporal discretization on the marching-on-in-time solution of integral equations is presented. Numerical results that quantify the efficiency–accuracy tradeoff for causal piecewise polynomial and band-limited interpolatory functions are presented. It is observed that the former is more efficient for low to moderate accuracy levels, and the latter achieves higher, but extrapolation-limited, accuracy levels.* © 2011 Wiley Periodicals, Inc. Microwave Opt Technol Lett 53:1343–1348, 2011; View this article online at wileyonlinelibrary.com. DOI 10.1002/mop.25960

1. INTRODUCTION

Time domain integral equation (IE) formulations solved under the marching-on-in-time (MOT) framework are promising methods for efficient analysis of transient scattering. Over the last decade, various fast algorithms [1, 2], implicit solvers [3], well-conditioned IE formulations [4, 5], accurate temporal discretization methods [6–8], and singularity treatment methods [9–12] have been proposed for improving classical MOT solvers. Although most of these developments mirror those for frequency-domain solvers, major differences arise because MOT solvers use subdomain temporal basis functions rather than entire-domain sinusoidal/Fourier basis functions to represent the time variation of currents and fields. Indeed, the choice of the temporal basis function plays a critical role in the accuracy and efficiency of the MOT solution. It dictates the interpolation, integration, and extrapolation errors and impacts the matrix-fill, memory, and time-marching costs (see Section 2 for precise definitions).

This letter investigates the accuracy–efficiency tradeoff encountered when choosing subdomain temporal basis functions by contrasting two prototypical ones: the causal piecewise polynomial interpolatory functions (CPPIFs) [1–3, 10], sometimes called shifted Lagrange interpolants [2, 10], and the band-limited interpolatory functions (BLIFs) based on approximate prolate spheroidal wave functions [6–8]. The relative merits of CPIFFs and BLIFs are examined by solving the combined-field IE (CFIE) for various transient scattering problems and measuring the accuracy and efficiency of the MOT solution. The CFIE is used because its MOT solution is stable for a wide range of parameters, even ones that cause large errors; thus, it allows a comprehensive comparison of the temporal basis functions.

The rest of the letter is organized as follows. Section 2 formulates the MOT solution of CFIE and analyzes the main sources of errors that directly depend on the temporal basis function. Section 3 presents numerical results and quantifies the accuracy–efficiency tradeoff. Section 4 presents the conclusions.

2. FORMULATION

This section first reviews the CFIE, its MOT solution, and the two classes of temporal basis functions. It then presents a detailed analysis of the relevant errors.